

Modified Algorithm for Surface Tension with Smoothed Particle Hydrodynamics and Its Applications

H.F.Qiang¹, F.Z.Chen¹ and W.R. Gao¹

Abstract: Based on smoothed particle hydrodynamics (SPH) method with surface tension proposed by Morris, this paper is intended to modify equations for surface tension by modifying normal and curvature with corrective smoothing particle method (CSPM). Compared with the continuum surface force (CSF) model for surface tension employed in the traditional SPH method, the accuracy in the present paper is much higher in terms of handling the problems with large deformation and surface tension. The reason is that in the traditional SPH method the deficiency of particles is near the boundary and sharp-angled areas, and it causes gross errors of curvature calculation. Via a semicircular problem the new method is tested, the factors affecting the accuracy of which are then investigated, including surface definition, normal calculation and curvature calculation and smoothing length in curvature calculation is also confirmed reasonable. Furthermore, evolution of a liquid drop under surface tension from initial square shape is simulated by the new method. Compared with Morris method and grid-based volume of fluid method, there is higher accuracy at sharp-angled areas and the final particle distribution is more homogeneous. Then, based on the modified algorithm, coalescence process of two oil drops in water under surface tension is simulated. The results show a good agreement with physical process. The method presented here is more applicable to solve the surface tension problems in both vacuum and multi-phase fluid involving density differences. Moreover, second breakup of an oil drop in water accelerated by an impulsive force is analyzed through simulation.

Keywords: surface tension method, smoothed particle hydrodynamics, CSPM, CSF, curvature

¹ Faculty of Mechanical & Propulsion Engineering, Xi'an Hi-Tech Institute, Xi'an, Shaanxi, PRC, PC 710025

1 Introduction

Surface tension, as an important property of liquid, plays a significant role in the formation of drops, coalescence of colliding drops, breaking up of colliding drops and so on. Many researchers have shown great interest in numerical simulation for it. In practice surface tension has been brought in many techniques. Some of these use simplifying assumptions to increase computational efficiency, making it difficult to include extra physical or chemical effects or complicated boundary conditions. And some methods are difficult to be extended to three-dimensional problems. For example, level set methods (LSM) (Sethian, 1996) can deal with large interfaces, however, exact conservation of mass is not guaranteed. Since the droplets' colliding involves large deformation of free surface, it is very difficult to track moving interfaces for traditional grid based methods such as finite element method (FEM). When the pinch-off happens, the deformable FEM is no longer useful. Although the volume of fluid (VOF) (Hirt and Nichols, 1981) method is still applicable, the accuracy and stability of numerical schemes are questionable. As the time accelerate, interfaces become illegible. An adaptive local grid refinement technique (Nikolopoulos, Nikas and Bergeles, 2009) is needed in order to increase the resolution around the interface which is more computationally expensive. Smoothed particle hydrodynamics (SPH) (Monaghan, 1992; Monaghan, 2005), as a full Lagrangian particle method, is used when fluid interfaces are advected with very little numerical diffusion. The SPH formalism readily accommodates extra physical and chemical effects and highly irregular, mobile or even deformable boundaries (Morris, 2000). This flexibility readily carries over into three-dimensional problems.

At present, two methods exist in traditional treatment of surface tension in SPH. One is imported from molecular interaction, using molecular cohesive pressure within van der Waals(vdW) model or intermolecular interactions to cope with the surface tension. Nugent and Posch(2000) applied the SPH method to van der Waals(vdW) fluid and studied the oscillation of a droplet with an initial rectangular shape under the surface tension. Although the surface tension generated by this method agrees well with the analytical solution, there still exists unphysical clustering in the simulation. Y. Meleán, L. D. G. Sigalotti and A. Hasmy(2004) removed the tensile instability by adding an artificial stress method and an energy generation term to the standard SPH equations. Y. Meleán and L. D. G. Sigalotti(2005) then employed the SPH method to simulate the coalescence of colliding van der Waals liquid drops and took the effects of different impact velocities on the collision of two drops into consideration. Unfortunately, the new method by Y. Meleán had to compromise between avoiding tensile instability and reproducing the van der Waals phase diagram. M. Y. Zhang, H. Zhang and L. L. Zhang(2006;

2009) avoided the particles clustering by using XSPH and studied the droplet impact on a smooth substrate in 3D with solidification. A. Colagrossi and M. Landrini(2003) increased the accuracy of interface by introducing molecular cohesive pressure within van der Waals(vdW) model as simulating the interface of two flows. G. Z. Zhou and Ge Wei(2008) introduced a repulsion between the neighboring particles of different fluids to arise surface tension automatically. The methods above for surface tension are all from molecular interaction and have a nature advantage over other numerical methods by which very complex interface tracking techniques are needed. However, they can not be used widely, for the parameters in the model can not correspond to macro parameters naturally.

The other method presented by Morris originally comes from continuum surface force (CSF)(Brackbill, Kothe and Zemach, 1992) model. Morris(2000) studied the theoretical computational process and simulated surface tension acting at an interface between two fluids of the same density and viscosity. The accuracy near the boundary or at sharp-angled areas is not taken into account, nor is the extension of the method to higher density and viscosity ratios yet concluded. M. Müller, D. Charypar and M. Gross(2003) attained a simpler method through initializing the color functions, the idea and solving process of which coincide with Morris's. H.S.Fang et al(2009) and Bao Kai et al(2009) simulated the evolution of a liquid drop under surface tension from initial square shape, spreading and solidification of a droplet with high impact Reynolds number and dam-break flow with the simpler method. Nevertheless the incompressible can't satisfy the request. The methods above all have gross errors in the curvature computation of those areas deficient in particles near the boundary and at the sharp-angled areas. The cases related to density differences are not involved and the factors affecting the surface tension are not recognized fully.

Corrective smoothed particle method (CSPM) was proposed by J.K.Chen(1999) who combined the kernel estimate with the Taylor series expansion in 1999. That algorithm resolves the general problem of particle deficiency at boundaries and improves the computational resolution, consistency and tensile instability effectively (Chen, Beraun and Carney, 1999; Chen and Beraun, 2000).

In this work, we modified the surface tension method based on SPH method with surface tension proposed by Morris. To raise the accuracy of surface curvature calculation at sharp curvature areas, the normal and curvature were revised with CSPM. Then higher curvature accuracy and more homogeneous particles distribution calculation were obtained. Furthermore, XSPH was used to smooth the velocity field. A semicircular problem was carried out to demonstrate the accuracy in surface defining, normal calculation and curvature calculation. The relationship of smoothing length between curvature formula and normal formula was also

analyzed. Two engineering tests on coalescence of two oil drops in water and secondary breakup of oil drop in water were simulated to prove the practicability in engineering of the new method.

2 CSF model

The CSF model interprets surface tension as a continuous, three-dimensional effect across the interface, rather than as a boundary value condition on the interface. The model is from defining a color function through which the normal and curvature are obtained. In this model, surface tension is translated into a force per unit volume. Conservation of momentum should be guaranteed exactly in this method.

In this paper we address the accurate modeling of the normal boundary for interfaces where the surface tension coefficient is constant and the interface thickness is limited. The force per unit volume, \mathbf{F}_s can be written as

$$\mathbf{F}_s = \mathbf{f}_s \delta_s \quad (1)$$

where δ_s is a normalized function that peaks at the interface and usually is chosen as surface delta function $|\mathbf{n}|$. \mathbf{f}_s is the force per unit area given by

$$\mathbf{f}_s = \sigma k(\mathbf{x}) \hat{\mathbf{n}} \quad (2)$$

where σ is the surface tension coefficient, $k(\mathbf{x})$ is the curvature of the interface at \mathbf{x} , and $\hat{\mathbf{n}}$ is the unit normal to the interface. The normal \mathbf{n} can be obtained by

$$\mathbf{n} = \frac{\nabla c(x)}{[\nabla c(x)]} \quad (3)$$

$c(x)$ is the color function identifying each fluid in the problem and $[\nabla c(x)]$ is the jump across the interface. The curvature is calculated through the formula

$$k = -(\nabla \cdot \hat{\mathbf{n}}) \quad (4)$$

3 The standard SPH equations

3.1 Governing equations

The fluids in this paper are considered as viscous and incompressible fluids with the heat transfer is neglected. The surface tension can't be ignored for droplets evolution and colliding. The governing equations are written in Lagrangian form as

$$\begin{cases} \frac{d\mathbf{v}}{dt} = -\frac{1}{\rho} \nabla P + \nu \nabla^2 \mathbf{v} + \mathbf{f}_s \\ \frac{d\mathbf{x}}{dt} = \mathbf{v} \end{cases} \quad (5)$$

where \mathbf{v} is particle velocity; t is time; ρ is fluid particle density; P is pressure; ν is kinematic viscosity; \mathbf{f}_s is surface tension; \mathbf{x} is particle position.

In order to describe the incompressible flow, it's necessary to use an artificial compressibility equation (Monaghan, 1994),

$$P = B \left[\left(\frac{\rho}{\rho_0} \right)^\gamma - 1 \right] + \chi \quad (6)$$

where B is reference pressure; γ denotes constant, usually, $\gamma = 7$; χ is background pressure, while $\chi = 0$ standing for free-surface flows. The parameters B, γ are chosen to have maximum density oscillations of order of $\vartheta(1\%)$. In practice, this is accomplished by choosing the sound speed 10 times or larger than the highest fluid velocity expected in the analyzed physical problems. There $B = 100\rho_0 v_{\max}^2 / \gamma$, where ρ_0 is the initial density of the fluid, v_{\max} is the maximum velocity.

When the incompressible fluid is considered as weakly compressible, the density ρ can not keep constant. Continuum equation in Lagrangian form is needed to compute density

$$\frac{d\rho}{dt} = -\rho \nabla \cdot \mathbf{v} \quad (7)$$

3.2 SPH formulations

In SPH method, the fluid is discretized by particles. The equations governing the evolution of fluid quantities are expressed as summation interpolations using a kernel function W with smoothing length h . The common differential SPH-based equations are, then, generated. These equations describe the varying of physical parameters and position of each SPH particle, the most usual one of which is the standard approach to SPH presented by Monaghan(1992). In this paper, we simulated two fluids of different density and viscosity. Due to the fact that numerical instability in the interface with density gradient may trigger the collapse of the computation, the modified SPH equations improved by Frank Ott and Erik Schnetter (2003) are adopted to deal with multi-phase flows effectively. Here we will utilize this modified equations.

As calculating viscous forces, one expression is from summing over particles with adding the computational effort. The other is directly from employing second derivatives of kernel. The disadvantage of using second derivative is that interpolation is much more susceptible to error at low resolution and hence, we use an SPH estimation of viscous diffusion which was firstly employed by Monaghan to model heat conduction and was also used by Morris(1997) to simulate the incompressible fluid at low Reynolds number. This hybrid expression is expressed to combine a

standard SPH first derivative with a finite difference approximation of a first derivative. Therefore the full SPH equations of multi-phase viscous flows can be written as

$$\begin{cases} \frac{d\rho_i}{dt} = m_i \sum_{j=1}^N \mathbf{v}_{ij} \cdot \nabla_i W_{ij} \\ \frac{d\mathbf{v}_i}{dt} = - \sum_{j=1}^N m_j \left(\frac{P_i + P_j}{\rho_i \rho_j} \right) \nabla_i W_{ij} \\ \quad + \sum_j^N m_j \frac{\mu_i + \mu_j}{\rho_i \rho_j} \mathbf{v}_{ij} \left(\frac{1}{r_{ij}} \frac{\partial W_{ij}}{\partial r_{ij}} \right) + \mathbf{f}_s \\ \frac{d\mathbf{x}_i}{dt} = \mathbf{v}_i \end{cases} \quad (8)$$

where $W_{ij} = W(\mathbf{x}_i - \mathbf{x}_j, h)$ is kernel function, which is important to numerical stability and accuracy. So far, the cubic spline function has been the most widely used smoothing function. h denotes the smoothing length. $\nabla_i W_{ij}$ denotes gradient kernel function. $\mathbf{v}_{ij} = \mathbf{v}_i - \mathbf{v}_j$, r_{ij} is the distance between particle i and j , $\mu = \rho\nu$ is the dynamic viscosity. Artificial viscosity is not needed in this paper for there is a realistic viscosity force and the flow is at low Weber number.

To improve the particle distribution during the movement in SPH, XSPH by Monaghan(1992) is generally used and the particle velocity is smoothed as follows

$$\frac{d\mathbf{x}_i}{dt} = \mathbf{v}_i - \varepsilon \sum_j \frac{m_j}{\bar{\rho}_{ij}} \mathbf{v}_{ij} W_{ij} \quad (9)$$

where $\varepsilon(0 \leq \varepsilon \leq 1)$ denotes a constant and its value of 0.3 is usually used. It makes the particles distribution more orderly by averaging its velocity with adjacent particles and the stability of the numerical simulation is usually improved.

4 Modified Algorithm for Surface Tension

As simulating the surface tension based on CSF model, the factors which affect the method accuracy should be held including surface definition, normal calculation and curvature calculation. We will investigate these factors next seriatim.

4.1 Defining surface

The defining of surface is related to the resolution of normal, even to that of curvature. Here, a standard interpolation expression(Morris, 2000) is smoothed as

$$\bar{c}_i = \sum_j \frac{m_j}{\rho_j} c_j W_{ij} \quad (10)$$

c_j is the color index of particle j , which is zero in the defined fluid field and one out the defined fluid field initially.

4.2 Modified normal with CSPM

The expression for \mathbf{n} derived by Monaghan(2000) with variational principles is given by

$$\mathbf{n}_i = \sum_j \frac{m_j}{\rho_j} c_j \nabla_i W_{ij} \quad (11)$$

There will be some unstable scatters some distance away from the interface when Eq.11 is used to compute curvature. In a dynamic simulation, these scatters disrupt the calculation. With a view to the phenomenon mentioned above, Morris(2000) improved the accuracy by smoothing the normal as

$$\mathbf{n}_i = \sum_j \frac{m_j}{\rho_j} (c_j - c_i) \nabla_i W_{ij} \quad (12)$$

This involves a difference between neighboring particle colors as a matter of which the accuracy is higher. In this paper, we modified Eq.11 with CSPM derived by J.K.Chen, and the main idea is to apply the corrective kernel estimate to the Taylor series expansion. The modified normal equations in three-dimensional (3-D) geometry are

$$n_{\alpha i} = \left[\sum_{j=1}^N (\bar{c}_j - \bar{c}_i) W_{ij,\beta} \frac{m_j}{\rho_j} \right] \left[\sum_{j=1}^N (x_j^\alpha - x_i^\alpha) W_{ij,\beta} \frac{m_j}{\rho_j} \right]^{-1} \quad (13)$$

where $\alpha, \beta=1, \dots, 3$, indicate spatial variables. $n_{\alpha i}$ is the normal vector at α direction of the particle i , \bar{c}_i and \bar{c}_j are obtained from Eq.10, $W_{ij} = W(\mathbf{x}_j - \mathbf{x}_i, h)$, $W_{ij,\beta} = \partial W_{ij} / \partial x_j^\beta$. The resolution is higher with this formula than Eq.12 in dealing with the deficiency of particles near the boundary. It is verified in section 5.1.

4.3 Modified curvature with CSPM

Curvature is the divergence of normalized normal. The traditional SPH expression(Morris, 2000) of curvature k is

$$k_i = -(\nabla \cdot \hat{\mathbf{n}})_i = -\sum_j \frac{m_j}{\rho_j} \hat{\mathbf{n}}_j \cdot \nabla_i W_{ij} \quad (14)$$

A more accurate estimation of divergence is obtained by Monaghan(2000) with

$$k_i = -(\nabla \cdot \hat{\mathbf{n}})_i = -\sum_j \frac{m_j}{\rho_j} (\hat{\mathbf{n}}_j - \hat{\mathbf{n}}_i) \cdot \nabla_i W_{ij} \quad (15)$$

However, for the normalized normal $\hat{\mathbf{n}}$ is small and have an erroneous direction along with the distance away from the interface, any estimate of curvature will be inaccurate. Morris(2000) suggested using $|\mathbf{n}|$ appropriate criteria to determine if a normal is “reliable” before including it in a divergence calculation. That is

$$N_i = \begin{cases} 1, & \text{if } |\mathbf{n}_i| > \xi \\ 0, & \text{otherwise} \end{cases} \quad (16)$$

and

$$\hat{\mathbf{n}}_i = \begin{cases} \mathbf{n}_i/|\mathbf{n}_i|, & \text{if } N_i = 1 \\ 0, & \text{otherwise} \end{cases} \quad (17)$$

When the normal value $|\mathbf{n}_i|$ is less than parameter ξ , the normal value and unit normal vector should be set zero, which is thought to have no effect on the curvature calculation. Typically, ξ is taken $0.01/h$. It is the same with modifying normal, the curvature is revised with CSPM. The modified divergence components of $\hat{\mathbf{n}}$ in three-dimensional (3-D) geometry are

$$\hat{n}_{\gamma,\alpha i} = \left[\sum_{j=1}^N (\hat{n}_{\gamma j} - \hat{n}_{\gamma i}) W_{i,j,\beta} \frac{m_j}{\rho_j} \right] \left[\sum_{j=1}^N (x_j^\alpha - x_i^\alpha) W_{i,j,\beta} \frac{m_j}{\rho_j} \right]^{-1} \quad (18)$$

which are brought in curvature equation

$$k_i = -(\nabla \cdot \hat{\mathbf{n}})_i = -\left(\frac{\partial \hat{n}_{xi}}{\partial x} + \frac{\partial \hat{n}_{yi}}{\partial y} + \frac{\partial \hat{n}_{zi}}{\partial z} \right) = \hat{n}_{x,xi} + \hat{n}_{y,yi} + \hat{n}_{z,zi} \quad (19)$$

where, $\alpha, \beta, \gamma=1, \dots, 3$, indicate spatial variables. $\hat{n}_{\gamma i}$ and $\hat{n}_{\gamma j}$ are normalized normal vectors at direction γ of particles i and j , which are obtained from Eq.17. $\hat{n}_{\gamma,\alpha i}$ is partial derivative at direction α of the normalized normal vector \hat{n}_{γ} of particle i . It is also verified in section 5.1.

Recently Adami, Hu and Adams(2010) derived a new reproducing divergence approximation to obtain a stable and accurate scheme for surface curvature. The approach is also based on the corrected kernel form proposed by Chen, but the differences are: our approach is proposed based on analyzing the deficiency of the method of Morris and it is tested through a semicircular problem. The factors affecting the accuracy are all investigated, including surface definition, normal calculation and curvature calculation and smoothing length in curvature calculation is also confirmed reasonable. Thus for improving the accuracy we also modified the normal with CSPM which was not done by Adami and co-authors. Otherwise, the formulas of surface tension force per unit mass on different occasions are obtained by analyzing.

4.4 The equation of surface tension per unit mass

For keeping the thickness of transition region a constant, Brackbill(1992) proposed fluid acceleration due to surface tension depended only on density gradients, not on the value of the density itself. The acceleration of an interface particle by surface tension \mathbf{f}_s in Eq.8 is

$$(\mathbf{f}_s)_i = -\frac{\sigma}{\langle \rho \rangle} (\nabla \cdot \hat{\mathbf{n}})_i \mathbf{n}_i \quad (20)$$

where, $\langle \rho \rangle = (\rho_0 + \rho_1)/2$, ρ_0, ρ_1 are the density of the fluids on both sides of the interface. For a single fluid case, Eq.20 is written as

$$(\mathbf{f}_s)_i = -\frac{2\sigma}{\rho_i} (\nabla \cdot \hat{\mathbf{n}})_i \mathbf{n}_i \quad (21)$$

For cases of two kinds of fluids on two sides of the interface, if Eq.20 was used to calculate the surface tension, each SPH particle on the interface would carry the same surface tension force. As a result, the interface would become very blurred. The analysis for the phenomenon is: FVM is an Euler method, while the interface is defined by the volume of fluid flowing into the grid of the interface. To keep the thickness of the transition region a constant, the surface force on both sides should be equal. However, for SPH is a full Lagrangian method, the interface tracking is related with the force on each particle. During calculation of the surface forces it must be ensured that the forces on both sides are not equal. Thus the interface can become clear and the two fluids are separated. So the equation of surface tension per unit mass for multi-phase fluids is

$$(\mathbf{f}_s)_i = -\frac{\sigma}{\rho_i} (\nabla \cdot \hat{\mathbf{n}})_i \mathbf{n}_i \quad (22)$$

4.5 Time integration

Here we used a leapfrog integrator (Monaghan, 1992) to update the position and velocity of the particles. It takes the form as follows

$$\phi_i(t + \delta t/2) = \phi_i(t - \delta t/2) + \phi_i(t) \delta t \quad (23)$$

$$x_i(t + \delta t) = x_i(t) + v_i(t + \delta t/2) \delta t \quad (24)$$

where ϕ indicates density ρ and velocity \mathbf{v} , \mathbf{x}_i is the position of particle i .

In quasi-compressible fluid, to maintain numerical stability with respect to surface tension force, the time step must be appropriate. This paper adopts a Courant-Friedrich-Lewy (CFL)(Monaghan, 1992) condition to estimate the time step. The

condition due to the maximum artificial sound velocity c_{\max} and maximum fluid velocity u_{\max} is

$$\Delta t \leq 0.25 \frac{h}{c_{\max} + |u_{\max}|} \quad (25)$$

The time step resolving the propagation of capillary waves (Brackbill, Kothe and Zemach, 1992) is

$$\Delta t \leq 0.25 \left(\frac{\rho h^3}{2\pi\sigma} \right)^{1/2} \quad (26)$$

The condition based on viscosity diffusion (Morris, Fox and Zhu, 1997) is

$$\Delta t \leq 0.125 \frac{\rho h^2}{\mu} \quad (27)$$

The gravitation does not influence the time step in this paper. Finally, we choose the minima during Eq.25, Eq.26 and Eq.27 as the time step in computation.

5 Numerical Tests

In this section, some numerical examples are given to test the new method derived above. In all cases we employ a cubic spline kernel (Monaghan, 1992) as the weighted function in the form

$$W(\mathbf{r}, h) = \frac{a}{h^v} \begin{cases} 1 - 1.5q^2 + 0.75q^3 & 0 \leq q \leq 1 \\ 0.25(2 - q)^3 & 1 \leq q \leq 2 \\ 0 & q > 2 \end{cases} \quad (28)$$

where $q = |\mathbf{r} - \mathbf{r}'|/h$, spatial dimension $v = 1, 2, 3$, accordingly the parameter $a = 2/3, 10/7\pi, 1/\pi$. For the compressible flows, $\gamma = 7.0$ is the ratio of specific heats. $\varepsilon = 0.3$ is in XSPH equation. In normal calculation $\xi = 0.01/h$.

The fluids in all tests are water and diesel oil. The parameters can be seen in Table 1. There the surface tension coefficient refers to two different types: one is the surface tension between the fluid and the air; the other one is the surface tension between the two different fluids.

5.1 Semicircular problem

For the purpose of testing the accuracy of the new method, we chose a semicircular problem in vacuum which contained linear boundary, curving boundary, sharp-angled areas and areas with particles deficiency initially. Choices of color function,

surface defining, surface normal calculation and curvature calculation are all investigated. The use of different levels of smoothing length to evaluate the curvature and the surface delta function is analyzed through comparing the numerical results. The initial particle distribution is shown in Fig.2. The number of particles is 361 and the distance $\Delta x = 5 \times 10^{-6}$ m. The smoothing length evaluating the curvature is denoted by H , the surface delta function by h which is also the smoothing length in SPH basic equations. During this test, it is all used that $H = 1.5h = 3\Delta x$ except for the graph in Fig.6(b) gained under the different times H is larger than h . (Fig.1, Fig.3 and Fig.4 are all three-dimensional for reflecting the function relationship. The numerical results are displayed on grid nodes through inverse-distance interpolating).

The surface is defined through color function in Eq.10, while the surface normal is from the new method of Eq.13. (See Fig.1 and Fig.2.) As are shown in the figures, the color function here is smooth and the surface normal is accurate. It can be seen from the formula $\hat{c} = 0.5(c_1 + c_2)$, the value of the color function on the surface is 0.5. The boundary line in Fig.2 is the contour of $c = 0.5$. From the figure we can see the surface attained from simulation agrees well with the true one and the normal is calculated accurately.

Fig.3 shows the curvature calculated by the method of Morris and Fig.4 is got by the new method. The curvature varies along the radius because the drop interface thickness is comparable to the radius of the drop. Through comparison it is proved the accuracy of curvature under the new method is larger meanwhile the curvature of other parts can also meet the requirement.

Table 1: Properties of diesel oil and water

Material	Density (kg/m ³)	Surface tension coefficient (N/m)	Surface tension coefficient between diesel oil and water (N/m)	Viscosity (Ns/m ²)
Diesel oil	819.0	0.02825	0.050475	3.16×10^{-3}
Water	1000	0.0727		1.002×10^{-3}

Fig.5 shows the specific particles used for testing some parameters. The particles selected for testing in Fig.6 are the ones filled with the black color. The accuracy with the new method modifying the normal is higher than that of not in both cases of the curvature modified (see Fig.6 (a)). It can not increase the computational price for the parameters used in modifying the normal and curvature are the same. Fig.6 (b) is the comparison of curvature when H is different from h . We can observe as H increases, the smoother curvature can be obtained. However, it has to pay more

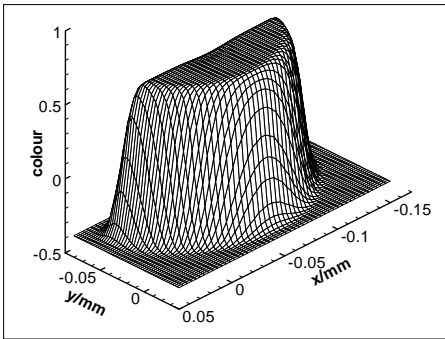


Figure 1: Color function

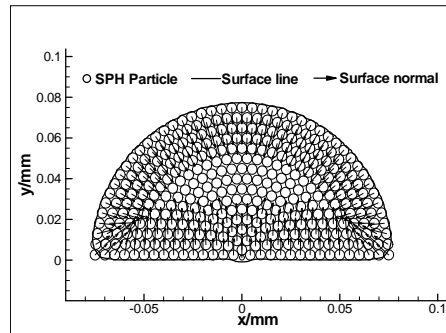


Figure 2: Surface and normal by the new method

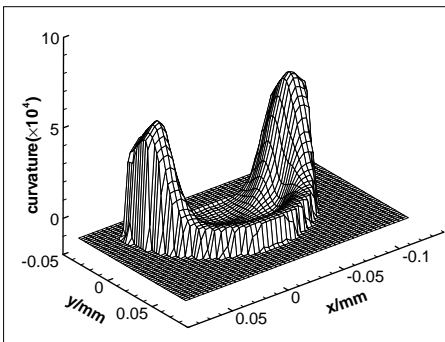


Figure 3: Curvature by the method of Morris

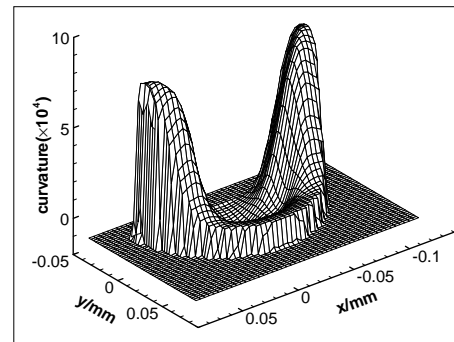


Figure 4: Curvature by the new method

computational price. A similar observation has already been made by S. Nugent et al (Nugent and Posch, 2000). The curvature at position (0.0, 0.0) is not zero for asymmetrical particles' distribution initially.

For describing more clearly the accuracy of the modified algorithm at areas of sharp-angled and with particles deficiency initially, on the basis of the above-mention tests of related parameters, we choose two particles at special areas (particle 1 at sharp-angled area and particle 2 at center of the semicircle (see Fig.5)) to analyze further the curvature. The results are shown in Tab.2. It can be seen through comparison the accuracy under the new method with both modifying the normal and curvature and the smoothing length $H=2.0h$ is more delicate than that of Morris and the interference is reduced at the areas with particles deficiency initially. But it increases the computational price at the same time. Although with both normal and curvature correction and the smoothing length $H=1.5h$ the interference

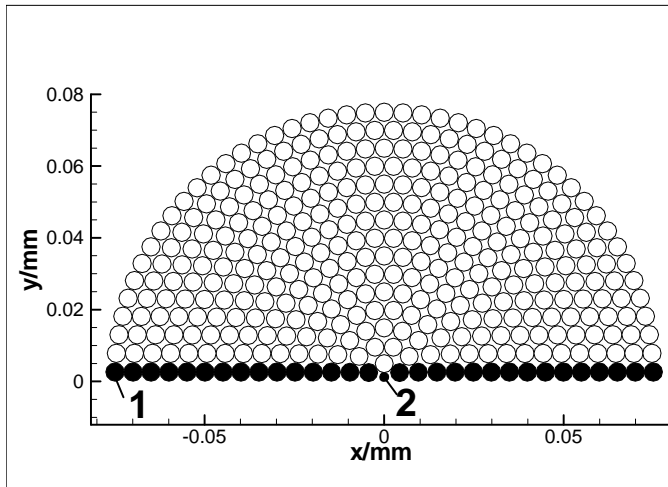
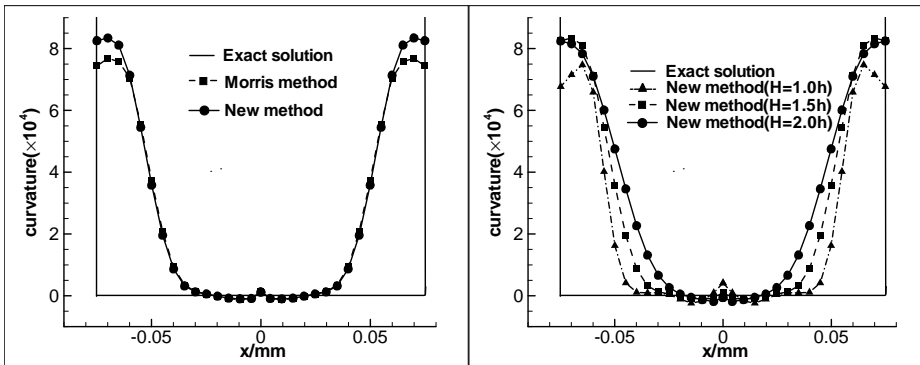


Figure 5: Particles used for testing some parameters in semicircular problem (The black particles are used to calculate the curvature in Fig.6 and particle 1 and particle 2 are used in Tab.2.)



(a) Curvature affected by modifying normal (b) Comparison of curvature when H is different from h

Figure 6: Comparison of curvature under different conditions

at the areas with particles deficiency initially is larger than that of Morris, the accuracy of curvature calculation is higher and the computational price is smaller. Thus, the smoothing length $H=1.5h$ is all used in the modified algorithm involved in later chapters examples.

Table 2: Curvature values at special points with different methods (The percentage shows the ratio of accuracy improved by different modified methods on the base of Morris.)

	Morris method	Curvature modified but normal not $H=1.5h$	Curvature and normal both modified $H=1.0h$
Curvature of particle 1($\times 10^4$)	4.38834	7.43848	6.77117
Percentage of the accuracy improved		69.5%	54.30%
Curvature of particle 2($\times 10^4$)	0.09004	0.14207	0.41249
	Curvature and normal both modified $H=1.5h$	Curvature and normal both modified $H=2.0h$	Theoretical value
Curvature of particle 1($\times 10^4$)	8.25619	8.244573	∞
Percentage of the accuracy improved	88.14%	87.87%	
Curvature of particle 2($\times 10^4$)	0.11805	0.059255	0

5.2 Evolution of an initially square shaped drop in vacuum

Surface tension always makes liquid surface constrict and the surface area is kept a minimum. The square droplets can contract and oscillate about its equilibrium shape. The droplet will keep circular evenly for viscosity dissipation, which is the reason why many liquid drops keep circular. The objective of this test is to validate the surface tension through comparing with Morris method and traditional grid based method. Simultaneously the periods of oscillation is obtained for supplying parameters and reliability index. The initial distribution of particles is 30×30 and the material is oil in vacuum. The parameters can be seen in Table 1. Fig.7-9 are the droplet's shapes at different time under three methods. They were all calculated through Eq.21. The solid line in Fig.9 is the boundary line of $c = 0.5$. It can be drawn through comparing the shape of the droplet in one cycle the particles in modified algorithm are more stable than that in Morris method and FVM-VOF method. The form of angular can be maintained when the drop vibrates to the limit state and the particles are in good order. Compared with the method of Morris, the

oscillation period of the new method is closer to the actual one and the accuracy is also higher. Simultaneity compared with FVM-VOF method, at the limit time the maximum of the drop at x direction of the new method can reach $9.45 \times 10^{-5}m$, however that of VOF method can only reach $8.865 \times 10^{-5}m$. Otherwise, the number of the drop oscillation times before it keeps steady is fewer than that of the new method. That's because for VOF methods the accurate evaluation of the geometrical properties of the interface such as curvature also need to be improved by other methods such as dynamic mesh-adaptive methods. However, as the value of the curvature at the cusp still can not reach the theoretical value, there is still relatively small gap between the oscillation period and the actual value. The algorithm will be improved and refined further next on the basis of this article.

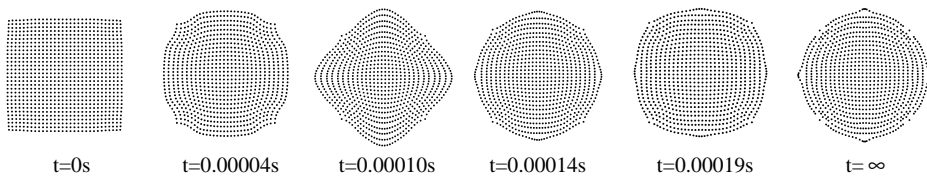


Figure 7: Square droplet's particles changing process under surface tension by Morris method

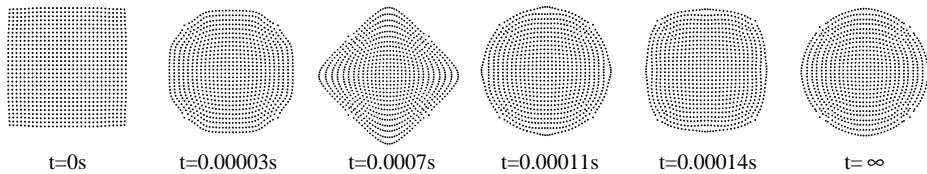


Figure 8: Square droplet's particles changing process under the new method

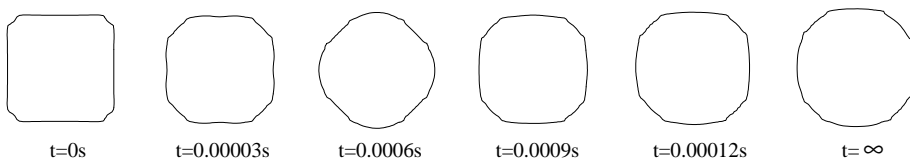


Figure 9: Square droplet's changing process under FVM-VOF method

5.3 Evolution of an initially square shaped oil drop in water in 2-D

For testing the feasibility of the new algorithm as it is used on the interface of two different fluids with density difference and supplying reliable basis for engineering applications, the square shaped drop is placed in a solution. The physical model is shown as Fig.10. That is an initially square shaped oil drop in water. The boundary with thickness $\Delta x = \Delta y = 25\mu m$ and particles number $n = 1420$, water with $\Delta x = \Delta y = 330\mu m$ and particles number $n = 3454$, and a square oil droplet with $\Delta x = \Delta y = 150\mu m$ and particles number $n = 900$.

Fig.11 and Fig.12 are the droplet's shape at different time under two methods. The finite volume method is found to coverage with 5774 cells spanning the initial square. The four time points are all the margin times in the periods. That is at 0.08ms the droplet contracted to a rhombus, then at 0.16ms it came back to square at the first time. Then the second period will continue until the kinetic energy is dissipated to zero by viscosity. The agreement between these two methods at the periods and shapes is excellent. For comparing the two methods comprehensively, the velocity fields at three typical times were chosen to be compared (see Fig.13 and Fig.14). It can be seen the two velocity vector plots are basically consistent. It is proved the process of calculation of the new method is correct.

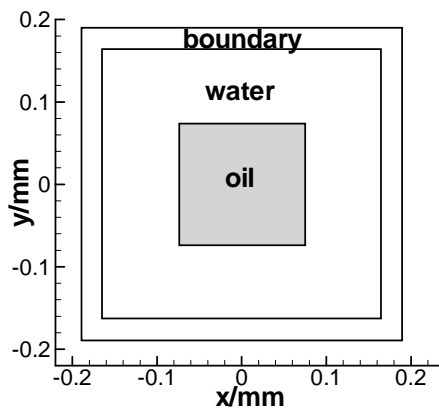


Figure 10: Physical model of test in section 5.3

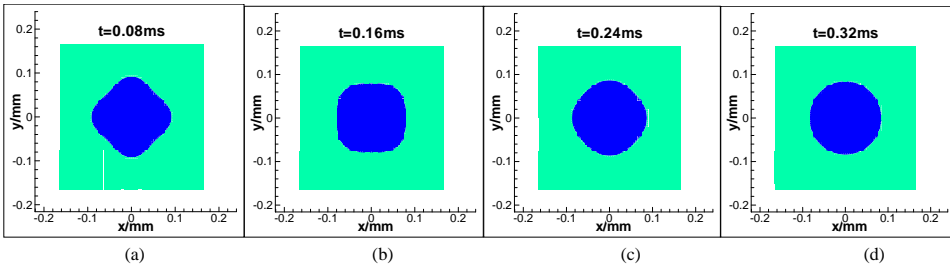


Figure 11: Square droplet’s changing process under FVM-VOF method

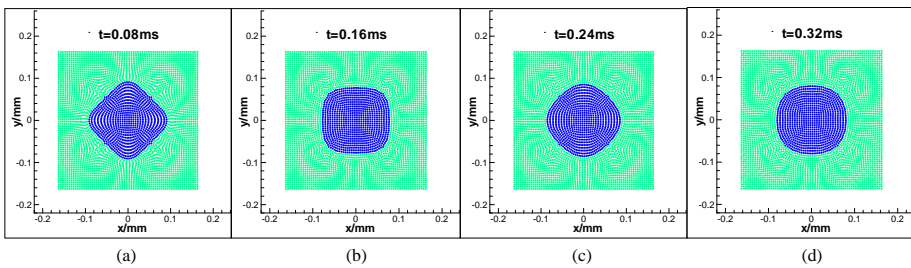


Figure 12: Square droplet’s particles changing process under the new method

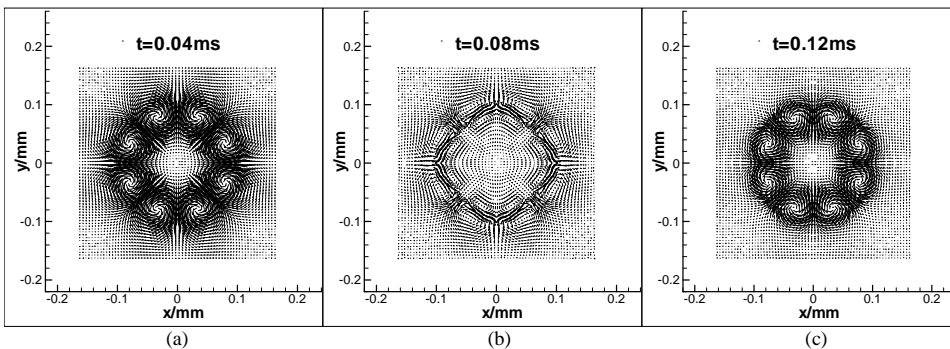


Figure 13: Square droplet’s velocity changing process under the new method

6 Engineering applications

6.1 Coalescence of two oil drops in water in 3-D

Coalescence of two small drops in liquid-liquid dispersions has appeared commonly in systems like latex preparation, liquid-liquid extraction, and separation with clarifying or multi-phase flowing in porous materials. It is significant to ap-

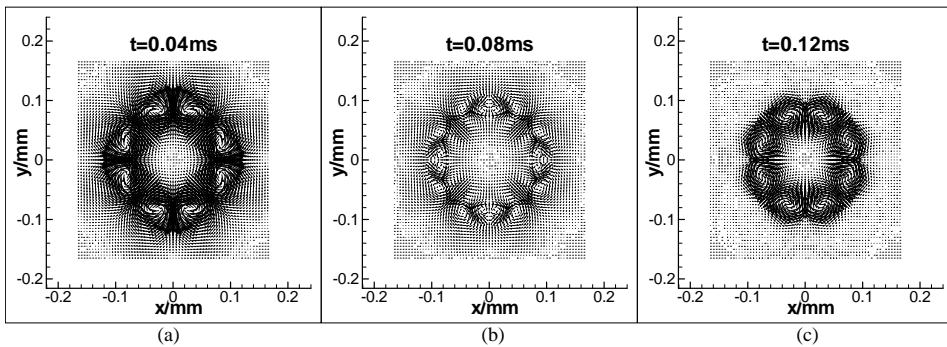


Figure 14: Square droplet’s velocity changing process under the FVM-VOF method

prehend and control the coalescence process. The test, coalescence of two oil drops in water, is simulated here. The parameters of oil and water can be seen in Tab.1. There are 110000 particles in all placed equidistantly in $x \in [-0.000140, 0.000140]$ $y \in [-0.0001025, 0.0001025]$ $z \in [-0.0001025, 0.0001025]$, and 1736 particles for each oil drop with diameter $D = 75\mu m$, 62624 particles for water. In Fig.15 we can see when two drops approach each other with no velocity initially, a dimpled thin liquid film is formed between them. As the liquid in film discharged, the interface can deform by the pressure changing. A dimpled film could be obtained along with thinnest areas occurred in film margins. The strong surface forces at high-curvature corners bring the drop into oscillation. Viscosity dissipation eventually damps the oscillation, causing the coalescence drop to approach an equilibrium spherical shape. The model simulating here predicts the coalescence time commendably.

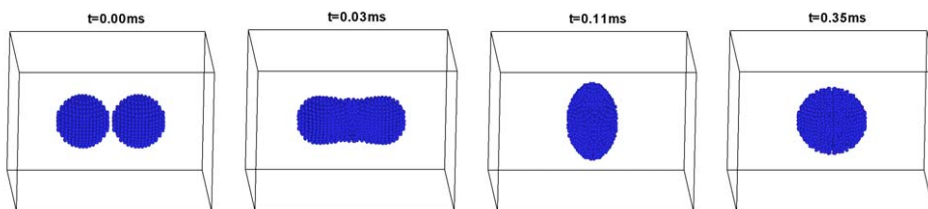


Figure 15: Deformation and coalescence of two oil drops in water of still state initially at four different times. At 0.03ms, the two drops combines completely and the film size is the same as the drop diameter. At 0.11ms, the film becomes thickest while the velocity filed is almost zero. The coalescence drop equilibrates to approach a spherical shape at about 0.35ms.

6.2 Secondary breakup of oil drop in water in 3-D

Secondary breakup is one of the stage processes in spray combustion, which can expand the total surface area of the fuel-air interface. The secondary breakup of drop has been widely investigated through experience (Chou and Faeth, 1998; Joseph, Belanger and Beavers, 1999; Dai and Faeth, 2001), while the simulation is less for its research and most of that is only on two-dimensions (2D). There are differences between two-dimensional simulation and three-dimensional simulation especially for oscillation breakup and bag breakup. Some three-dimensional numerical experiments of the secondary breakup of drop are operated exploringly in this text. It can be concluded through previous experiences: the effects of liquid viscosity can be negligible when $Oh < 0.1$; with low Weber number the drop do not break up with only deformation; as the acceleration increases past a critical value, the drops become progressively flatter and eventually break up. As the Weber number is increased, there are four different typical breakup modes (Han and Tryggvason(1999, 2001):

- (1) Oscillation breakup. The drop decomposes into several two or more equal-sized smaller drops.
- (2) Bag breakup. The original drop deforms into a torus-shaped rim spanned by a thin fluid film that ruptures into tiny droplets, followed by disintegration of the rim into larger droplets.
- (3) Shear breakup. Small drops are continuously stripped off the rim of the original drop.
- (4) Explosive breakup. The strong surface waves disintegrate the drop in a violent manner.

Three types of breakup (forward-facing bag breakup, backward-facing bag breakup and shear breakup (see Fig.17-19)) have been got through changing the density ratio and the drop velocity. The processes of the drop deformation are in line with the physics. For there is less experimental data on such problems and it's difficult for us to do such experiments, comparisons with the experiments have not been done. It's only used for testing the practicability in large deformation processes and related engineering fields. The simulation is subject to further experimental verification. In this text we take the secondary breakup of oil drops in water accelerated by an impulsive force into consideration. The drop of size $D = 75\mu m$ is located in a cuboid channel of size $L_x = 380\mu m$, $L_y = L_z = 155\mu m$ (see Fig.16). There are no-slip wall boundaries with thickness $\Delta x = \Delta y = 15\mu m$ and particles number $n = 39104$. The oil particles number is 1736 and water 46260. As it's shown at (Han and Tryggvason(1999, 2001), the Weber number, Ohnesorge number, density ratio and viscosity ratio affect the breakup mode and deformation rate. These are defined

by

$$We = \frac{\rho_0 v_{rel}^2 D}{\sigma}, \quad oh_d = \frac{\mu_d}{\sqrt{\rho_d D \sigma}} = \frac{\sqrt{We}}{Re}, \quad \gamma_p = \frac{\rho_d}{\rho_0}, \quad \gamma_\mu = \frac{\mu_d}{\mu_0} \quad (29)$$

Here, D is the initial diameter of the drop and v_{rel} is the initial relative velocity between the drop and the ambient fluid. The subscripts d, o denote the properties of the oil drop and water. Fig.17-19 show the deformation and breakup of oil drop in water at two different times.

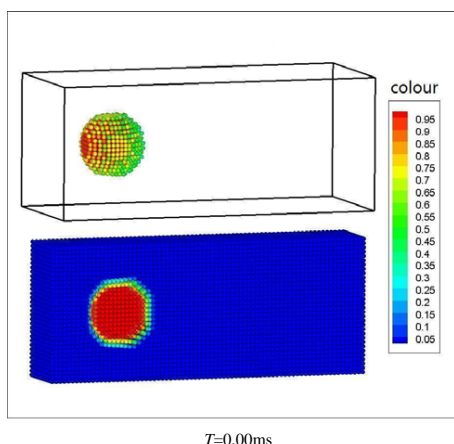


Figure 16: The initial form of the drop and the flow field in the secondary breakup. At each figure the above one is the deformation and breakup of oil drop spatially, while the below one is the sectional image of second breakup process in the y direction where the color denotes the value of the color function.

7 Conclusions

One of the traditional surface tension methods simulating surface tension is from microcosm perspective taking molecular cohesive or repulsive force into consideration, the parameters of which can not keep consistency with practicality in simulation. Simultaneously the accuracy at areas with small curvature is very low, thus the reflexive separation into two or more drops cannot be attained. The other one is based on CSF model from macro angel which simulates the surface tension directly. Although this method avoids the disadvantage of the microcosmic method, the curvature calculation of areas with deficiency of particles such as near the boundary and sharp-angled areas is not involved. As a result, the accuracy of the curvature is also very low.

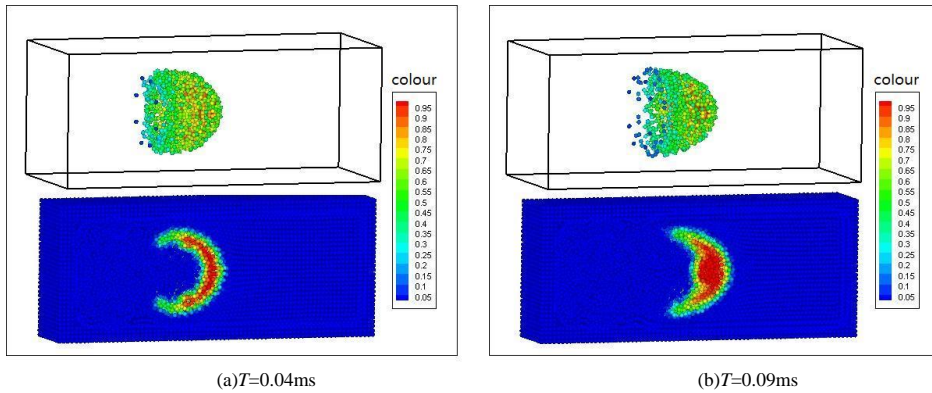


Figure 17: The forward-facing bag breakup process ($We = 47.54$, $oh_d = 0.057$, $\gamma_p = 1.638$, $\gamma_\mu = 3.16$)

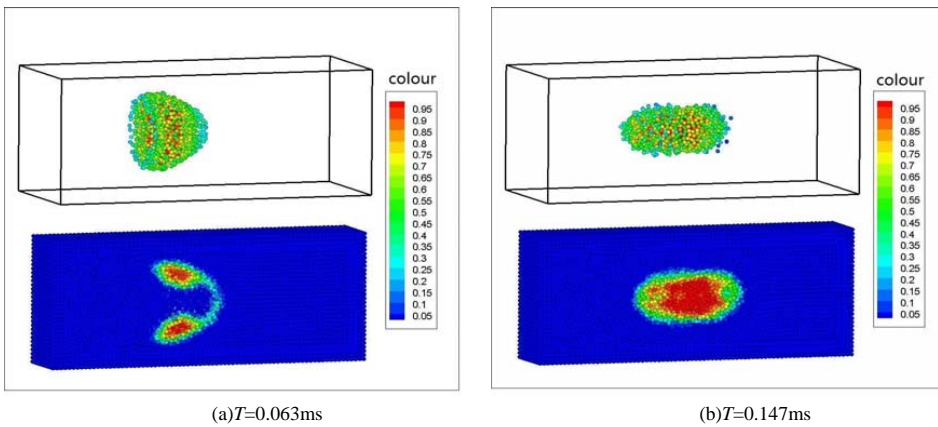


Figure 18: The backward-facing bag breakup process ($We = 95.09$, $oh_d = 0.057$, $\gamma_p = 0.819$, $\gamma_\mu = 3.16$)

This paper presents a new method to cope with surface tension which starts from CSF model based on SPH method with surface tension proposed by Morris. The modified equations for surface tension are derived by modifying normal and curvature with CSPM which can resolve the boundary deficiency problem and improve the tensile instability effectively (Chen, Beraun and Jih(1999)). The color function, normal calculation and curvature calculation all have been analyzed through numerical simulation. Through a typical test in surface tension simulations, evolution of a diesel oil in vacuum and in water from an initial square shape in 2-D,

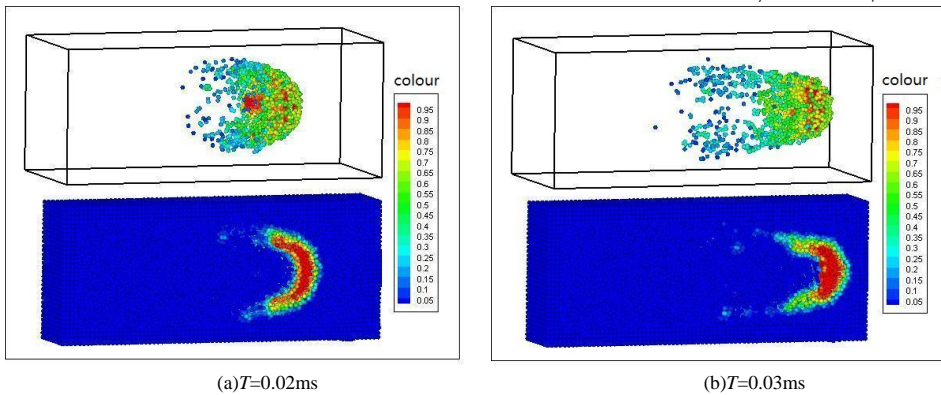


Figure 19: The shear breakup process ($We = 27.38$, $oh_d = 0.057$, $\gamma_\rho = 10$, $\gamma_\mu = 31.6$)

it's proved that the new method is feasible for solving such problems and the stability and accuracy are much higher comparing with Morris method and traditional grid based method (FVM-VOF), with supplying related parameters for engineering applications. The two engineering applications both display the capabilities of the new method in handling multi-phase and large deformation problems.

Acknowledgement: The support of New Century Excellent Talents in University (NCET), No. 613102 for National 973 Program in China and the Innovative Research Project of Xi'an Hi-tech Institute (EPXY0806) are gratefully acknowledged.

References

- Adami, S.; Hu, X. Y.; Adam, N. A.** (2010): A new surface tension formulation for multi-phase SPH using a reproducing divergence approximation. *Journal of Computational Physics*, vol. 229, pp. 5011-5021.
- Bao, K.; Zhang, H.; Zheng, L. L.; Wu, E. H.** (2009): Pressure corrected SPH for fluid animation. *Computer Animation and Virtual Worlds*, vol. 20, pp. 311-320.
- Brackbill, J. U.; Kothe, D. B.; Zemach, C.** (1992): A continuum method for modeling surface tension. *Journal of Computational Physics*, vol. 100, pp. 335-354.
- Chen, J. K.; Beraun, J. E.** (2000): A generalized smoothed particle hydrodynamics method for nonlinear dynamic problems. *Comput. Methods Appl. Mech. Engrg.*, vol. 190, pp. 225-239.

- Chen, J. K.; Beraun, J. E.; Carney, T. C.** (1999): A corrective smoothed particle method for boundary value problems in heat conduction. *International Journal for Numerical Methods in Engineering*, vol. 46, pp. 231-252.
- Chen, J. K.; Beraun, J. E.; Jih, C. J.** (1999): Completeness of corrective smoothed particle method for linear electrodynamics. *Computational Mechanics*, vol. 24, pp. 273-285.
- Chou, W. -H.; Faeth, G. M.** (1998): Temporal properties of secondary drop breakup in the bag breakup regime. *International Journal of Multiphase Flow*, vol.24: 889-912.
- Colagrossi, A.; Landrini, M.** (2003): Numerical simulation of interfacial flows by smoothed particle hydrodynamics. *Journal of Computational Physics*, vol. 191: 448-475.
- Dai, Z; Faeth, G. M.** (2001): Temporal properties of secondary drop breakup in the multimode breakup regime. *International Journal of Multiphase Flow*, vol.27: 217-236.
- Fang, H. S.; Bao, K.; Wei, J. A.; Zhang, H.; Wu, E. H.; Zheng, L. L.** (2009): Simulations of droplet spreading and solidification using an improved SPH model. *Numerical Heat Transfer, Part A: Applications*, vol. 55, pp. 124-143.
- Frank Ott, Erik Schnetter.** (2003): A modified SPH approach for fluids with large density differences. *Physics/0303112*.
- Gray, J. P.; Monaghan, J. J.; Swift, R. P.** (2001): SPH elastic dynamics. *Comput. Methods Appl. Mech. Engrg.*, vol. 190, pp. 6641-6662.
- Han, J.; and Tryggvason, G.** (1999): Secondary breakup of axisymmetric liquid drops. I. Acceleration by a constant body force. *Physics of Fluids*, vol. 11, pp. 3650-3667.
- Han, J.; and Tryggvason, G.** (2001): Secondary breakup of axisymmetric liquid drops. II. Impulsive acceleration. *Physics of Fluids*, vol. 13, pp. 1554-1565.
- Hirt, C. W.; Nichols, B. D.** (1981): Volume of fluid methods for the dynamics of free boundaries. *Journal of Computational Physics*, vol. 39, pp. 201-225.
- Joseph, D. D.; Belanger, J.; Beavers, G. S.** (1999): Breakup of a liquid suddenly exposed to a high-speed air stream. *International Journal of Multiphase Flow*, vol. 25, pp. 1263-1303.
- Meleán, Y.; Sigalotti, L. D. G.** (2005): Coalescence of colliding van der Waals liquid drops. *International Journal of Heat and Mass Transfer*, vol. 48, pp. 4041-4061.
- Meleán, Y.; Sigalotti, L. D. G.; Hasmy, A.** (2004): On the SPH tensile instability in forming viscous liquid drops. *Computer Physics Communications*, vol. 157, pp.

191-200.

Monaghan, J. J. (1992): Smoothed particle hydrodynamics. *Annual Review of Astronomy and Astrophysics*, vol. 30, pp. 543-574.

Monaghan, J. J. (1994): Simulation Free Surface Flows with SPH. *Journal of Computational Physics*, vol. 110, pp. 399-406.

Monaghan, J. J. (2000): SPH without a tensile instability. *Journal of Computational Physics*, vol. 159, pp. 290-311.

Morris, J. P. (2000): Simulating surface tension with smoothed particle hydrodynamics. *International Journal for Numerical Methods in Fluids*, vol. 33, pp. 333-353.

Morris, J. P.; Fox, P. J.; Zhu, Y. (1997): Modeling Low Reynolds Number Incompressible Flows Using SPH. *Journal of Computational Physics*, vol. 136, pp. 214-226.

Müller, M.; Charypar, D.; Gross, M. (2003): Particle-based fluid simulation for interactive applications. *Proceedings of Symposium on Computer Animation 2003*, pp. 154-159.

Nikolopoulos, N.; Nikas, K. -S.; Bergeles, G. (2009): A numerical investigation of central binary collision of droplets. *Computer & Fluids*, vol.38, PP. 1191-1202.

Nikolopoulos, N.; Nikas, K. -S.; Bergeles, G. (2009): Off-centre binary collision of droplets: A numerical investigation. *International Journal of Heat and Mass Transfer*, vol. 52, PP. 4160-4174.

Nugent, S.; Posch, H. A. (2000): Liquid drops and surface tension with smoothed particle applied mechanics. *Physical Review E*, vol. 62, pp. 4968-4975.

Sethian, J. A. (1996): Level Set Methods: Evolving Interfaces in Geometry, Fluid Mechanics, Computer Vision, and Materials Science. *Cambridge University Press: Cambridge*.

Zhang, M. Y.; Zhang, H.; Zheng, L. L. (2006): Smoothed particle hydrodynamics method for droplet instability, impact and solidification. AIAA, San Francisco, California.

Zhang, M. Y.; Zhang, H.; Zheng, L. L. (2009): Numerical investigation of substrate melting and deformation during thermal spray coating by SPH method. *Plasma Chem Plasma Process*, vol. 29, pp. 55-68.

Zhou, G. Z.; Ge, W.; Li, J. H. (2008): A revised surface tension model for macro-scale particle methods. *Powder Technology*, vol. 183, pp. 21-26.